Effect of Thermobaricity, Surface Buoyancy on Geostrophic Turbulence

Mo Rokibul Islam

PhD Proposal

Department of Atmospheric and Oceanic Science

McGill University

Montreal,Quebec

2016-07-21

TABLE OF CONTENTS

LIST OF TABLES

LIST OF FIGURES

Figure page

CHAPTER 1
Introduction

Fluid motion, including waves and turbulence, in the atmosphere and oceans can to a good approximation be thought of as a superposition of balanced and unbalanced flows. Balanced flows are slowly varying (time scales of 10 hours and longer) whereas unbalanced flows evolve more quickly. The term balance refers to an approximation to the horizontal momentum equation in which (fast) time derivative terms are ignored. The simplest and most widely used example is the quasi-geostrophic (QG) approximation, in which the leading order momentum balance has the horizontal pressure gradient and Coriolis forces summing to zero.

The theories of geostriphic turbulence ([3] ,[8],[7]) suggest that energy enters at large scales in the baroclinic mode and undergoes a direct cascade to the deformation radius-like scale where both baroclinic and barotropic modes are excited. Energy then transfer from baroclinic to bartrophic mode and undergoes an inverse cascade in the barotropic mode until it is removed through large scale dissipation, such as bottom friction. The β effect may also alter this isotropic view of the barotropic inverse cascade at large scales. This scenario, referred is called "dual cascade", is summarized in Figure 1–1. How this classical picture can be modified by the other factors like thermobaricity and vertical structure of jets in β-plane turbulence, we will be looking at this in next two Chapters.

Thermobaricity arise from nonlinear equation of state breaks conservation of potential vorticity (PV) even without viscous and dissipation effect. Balance dynamics is strongly connected to potential vorticity. Due to nonconserveness of enstrophy,

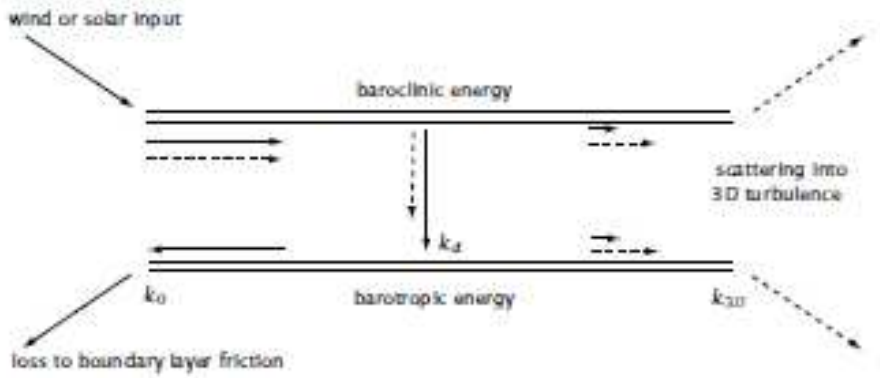

Figure 1–1: Schematic of the "dual cascade" view of energy transfers in baroclinic turbulence [8]. Energy enters at large scale in the baroclinic mode. There is a direct cascade of energy in the baroclinic mode. Transfer to the barotropic mode occurs near the deformation radius through baroclinic instability. Energy then undergoes an inverse cascade in the barotropic mode until it is removed through large scale dissipation, such as bottom friction.

energy may allow to move to down scales. This is important since in QG turbulence, energy dissipation is dominated by bottom friction at large scale. In Chapter 2, a modified version of QG (MQG) is proposed to analyze how thermobaricity interrupts those classical picture.

Dynamics of zonal jets in many previous studies has been evaluated from baroropic flow. The introduction of β also modifies, Figure 1–1, the isotropic view of the barotropic inverse cascade at large scales but this scales are not well defined. Recently, vertical structure of jets is observed. Now, question arises, does this vertical structures of jets effect the scales? Surface quasigeostrophic (SQG) dynamics and β plane turbulence with vertical structure will be discussed in Chapter 3.

CHAPTER 2
Modeling Thermobaric Effect on Quasigeostropihic Dynamics in the Ocean

2.1 Introduction

The equation of state of sea water is an empirical relationship between density ρ, pressure p temperature θ and salinity s. It is high nonlinear, but mainly two features are important: cabbeling and thermobaricity. Although, cabbeling plays an important role in the ocean, only the thermobaric effect would be discussed in this chapter.

The word *Thermobaricity* was first introduced by McDugall [11]. *Thermo* means temperature and *baric* means pressure and it relates to compressibility of sea water depending on pressure, temperature and salinity, however, dependency of salinity is weak. Because of thermobaric effect, a nonconservation arises in the Ertel's potential vorticity even without viscous and dissipation effect. This is an interest of balance dynamics, since balance dynamics is strongly link to potential vorticity. Here, we have considered this in quasigeostrophic (QG) context and are proposing a modified version of QG (MQG) that takes into account thermobaric effects. The MQG equations include an advection-diffusion equation for "spice"; that is, for the temperature-salinity composition of the water. Details will be discussed in Section 2.3.

Lateral variability of spice affects the base state buoyancy frequency $N^2(x, y, z, t)$, which can no longer be thought of as a function of z alone. Because of this, the three dimensional elliptic inversion cannot be separated into two dimensional inversions

for each vertical mode. A three dimensional multigrid method is used to solve the elliptic equation.

Straub [2] suggested by his scale analysis that the thermobaricity can lead to $O(1)$ changes in the vorticty distribution at the high wave number end of the spectrum and also can effect large scale flow. He also suggests that it may be unimportant in the upper ocean but may not be true in the deep ocean.

Thermobaricity is important for the studies of convection in deep oceans [6] such as Weddell Sea. Also, this effect is important at fronts between water masses in the world's oceans.

A numerical technique for MQG to handle this, as well as results are presented in Section 2.4.

2.2 Equation of State and Thermobaricity

The equation of state specifies the density ρ is a function of pressure p, potential temperature θ, and salinity s

$$\rho = f(p, \theta, s) \tag{2.1}$$

The orientation of the isopycnal in a $\theta - S$ diagram changes with pressure with a slope m,

$$m = \frac{\gamma \partial s}{\varphi \partial \theta} \tag{2.2}$$

where $\varphi = -\frac{1}{\rho}\frac{\partial f}{\partial \theta}$, $\gamma = \frac{1}{\rho}\frac{\partial f}{\partial s}$ are the thermal (φ)and haline (γ) expansion coefficients respectively. The change of the slope from one pressure level to another level

$$\frac{\partial m}{\partial p} = 2mb \tag{2.3}$$

where

$$b = \frac{1}{2}\left(\frac{1}{\gamma}\frac{\partial \gamma}{\partial p} - \frac{1}{\varphi}\frac{\partial \varphi}{\partial p}\right) \tag{2.4}$$

It is known that $\frac{\partial f}{\partial p} = \frac{1}{c^2}$, therefore, the change of slope is related to the dependence of sound velocity c. The physical meaning of changing in slope is, having same density of two fluid particles at a pressure level will differ at another level. This pressure dependency in equation of state is called thermobaricity.

The potential density σ is

$$\sigma = g(p_{ref}, \theta, s) \tag{2.5}$$

in a reference pressure p_{ref}. As σ does not vary with p, therefore, $\frac{\partial m}{\partial p} = 0$ as $b = 0$, implies that σ referenced to one pressure can be written as a function of σ referenced to another. In general, there is no reason to expect $b = 0$.

2.3 Modified Quasigeostrophic (MQG) Approximation

As we are considering pressure dependency, then the buoyancy frequency is

$$N^2 = \frac{g}{\rho_0}\frac{d\bar{\rho}(z)}{dz} - \frac{g^2}{c^2} \tag{2.6}$$

Here, $\bar{\rho}(z)$ is the base state stratification. We can separate c as a function of z and (x, y, z), $[c \approx c_0(z) + c_1(x, y, z)]$ and the base state buoyancy frequency can be written as [2]

$$N^2(x, y, z, t) = N_0^2(z) + N_1^2(x, y, z, t) = (1 + \alpha)N_0^2 \tag{2.7}$$

where

$$N_0^2 = \frac{g}{\rho_0}\frac{d\bar{\rho}}{dz} - \frac{g^2}{c_0^2}, \quad N_1^2 = \frac{2g^2}{c_0^2}\frac{c_1}{c_0}$$

The ratio (α) of N_1^2 and N_0^2 is a nondimentional parameter that measures the importance of thermobaricity. This parameter α is usually considered small, but can be large compared to the Rossby number (Ro), particularly near water mass boundaries in the abyssal ocean [2].

The governing equations for MQG are: the vorticity, the buoyancy and the spice equations are respectably

$$\frac{D}{Dt}\nabla^2\psi = f_0\frac{\partial w}{\partial z} + F \tag{2.8}$$

$$\frac{D}{Dt}b + w\left[N_0^2(z) + N_1^2(x,y,z,t)\right] = 0, \tag{2.9}$$

$$\frac{D}{Dt}N_1^2 = F_s, \tag{2.10}$$

where F and F_s are forcing term for vorticity and spice respectively and $\frac{D}{Dt}$ is 2-D total derivative. After doing a little algebra, we can rewrite the standard form of QG potential vorticity, Q_0, for MQG;

$$\frac{D}{Dt}Q_0 = -f_0\frac{\partial}{\partial z}\left(w\alpha\right) + F \tag{2.11}$$

where $Q_0 = \nabla^2\psi + \frac{f_0}{N_0^2}\frac{\partial b}{\partial z}$. Thermobaricity introduces a additional forcing term $f_0\left(w\alpha\right)_z$. Using chain rule, we get $\left(w\alpha\right)_z = w\alpha_z + w_z\alpha$ and can be scaled

$$w\alpha_z \sim \frac{w_0\alpha_0}{h}, \quad \alpha w_z \sim \frac{w_0\alpha_0}{H}$$

where α_0 and w_0 are typical values of α and w, and h is the vertical scale of spice. Therefore, $w\alpha_z$ is the dominant term and spice forcing would be scale like α_z. So, the net effect of this forcing [2];

$$\frac{\Delta Q_0}{Q_0} \sim \frac{\alpha_0 H}{h} \tag{2.12}$$

where ΔQ_0 is the net change in potential vorticity . Thus, we can expect $O(1)$ change in Q_0 when h becomes small compared to vertical scale of the flow H. As spice has small scale vertical structure and PV is forcing by spice, so, same structure should be observed in PV field.

The ω equation for w is

$$\nabla^2\left(N^2 w\right) + f^2 w_{zz} = N^2\nabla^2 w + w\nabla^2 N^2 + 2\nabla\cdot(wN^2) + f^2 w_{zz} = f(x,y,z) \quad (2.13)$$

Once horizontal length scale l of the spice moves forward to smaller than length scale L by advection, then the term, $w\nabla^2 N^2$, will large and effective. That suggest that spice may add more small horizontal scale phenomena.

2.3.1 Energy and Potential Enstrophy

Multiplying the equation (2.11) by Q_0 and integrate over volume, we get the potential enstrophy equation

$$\frac{\partial}{\partial t} Z_0 = \underbrace{Q_0 J(\psi, Q_0)}_{NL_{ens}} + \underbrace{f_0 \int Q_0 \frac{\partial}{\partial z}(w\alpha)\, dV}_{S_{ens}} + \underbrace{\int Q_0 F dV}_{F_{ens}}, \quad (2.14)$$

and multiplying the equation (2.11) by ψ and integrate over volume, the energy equation is obtained

$$\frac{\partial}{\partial t} E_0 = \underbrace{\psi J(\psi, Q_0)}_{NL_{en}} + \underbrace{f_0 \int \psi \frac{\partial}{\partial z}(w\alpha)\, dV}_{S_{en}} + \underbrace{\int \psi F dV}_{F_{en}} \quad (2.15)$$

where $E_0 = \int \left(\psi_x^2 + \psi_y^2 + \frac{f_0}{N_0^2} b^2\right) dV$ is total energy and $Z_0 = \int Q_0^2\, dV$ is enstrophy. Both energy and potential enstrophy are not conserved in MQG. Therefore, when the vertical length scale h of spice is small, α_z becomes important in both cases in PV field.

2.4 Numerical Simulations

2.4.1 Numerical Procedure

The barotropic $\bar{\psi}$ of ψ has been calculated from the vorticity equation (2.8) by imposing the following condition;

$$\nabla^2 \bar{\psi}_t + \overline{J\left(\psi, \nabla^2 \psi\right)}^z = 0 \tag{2.16}$$

where the ($^-$) represent the vertically averaged nonlinear part. And, the baroclinic part of ψ has been calculated from the buoyancy equation (2.9).

Vertical velocity of w have been calculated by solving a three dimensional elliptic equation ($\omega-$equation)

$$\nabla^2 \left(N^2 w\right) + f_0^2 \frac{\partial^2 w}{\partial z^2} = \nabla^2 \left(J(\psi, b)\right) + \frac{\partial}{\partial z}\left(J(\psi, \nabla^2 \psi)\right) + f \frac{\partial F}{\partial z} \tag{2.17}$$

As the lateral variability of spice affects the base state buoyancy frequency N^2, and we can not separate 3D elliptic inversion into 2d inversions for each vertical mode. So, we need a reliable numerical technique to solve full this 3D elliptic problem. To solve both 2D and 3D elliptic operators, multigrid numerical technique has been performed.

2.4.2 Parameter and Conditions

The horizontal domain sizes are $L \sim 4L_d$; where $L_d = \frac{NH}{f}$ is Rossby reformation radius. The Coriolis parameter is $f = 10^{-4} s^{-1}$, the base state buoyancy frequency is $N_0 = 50 \times f\ s^{-1}$, and vertical domain size is $H \approx 1.5km$. The vertical resolution must satisfy $\delta z \sim \frac{f \delta x}{N_0}$ to maintain stability in a numerical simulation of geostrophic flows [9]. A periodic boundary condition is used for horizontal direction. For the time integration, a second order leapfrog time-stepping scheme is used and a widely used $Robert - Asselin$ time filter is considered 0.1.

Run	$Nx \times Ny \times Nz$	F_s
1	$128 \times 128 \times 32$	0
2	$128 \times 128 \times 32$	$1F_s$
3	$128 \times 128 \times 32$	$2F_s$
4	$128 \times 128 \times 32$	$3F_s$
5	$128 \times 128 \times 32$	$4F_s$
6	$128 \times 128 \times 32$	$5F_s$

Table 2–1: Computational conditions for simulations

The computational grid 124 in each horizontal direction and 32 in vertical direction are used. The forcing is injected at the wavenumber $\kappa \approx 2$ horizontally and the first barcoclinic mode is used for vertical (z) direction and where as for spice $F_s = A\cos(\pi z)\sin(2\pi x)\sin(2\pi y)$ are considered, where $\kappa = \sqrt{k_x^2 + k_y^2}$ and A is the amplitude of spice forcing. We have six (6) simulations, $Run-1$ is standard QG simulation so $F_s = 0$, and from $Run-2$ to $Run-5$ are MQG simulation where A is increased by a addition factor of 1.

2.4.3 Spice

Forcing for spice has been increase a factor of one in our simulations from $Run-2$ to $Run-6$. Figure 2–1(a) describes the root mean square of spice with time and normalized by N_0^2 and a linear contribution of forcing is observed. Therefore, the simulations form 2 to 6 represent that $\alpha = \frac{N_1^2}{N_0^2}$ is about 0.04, 0.08, 0.12, 0.16, and 0.20 respectively and particularly, F_s is approximately 4% of total N_0^2.

2.4.4 PV Field

We put the forcing at large scale, so, initially spice work as a passive tracer. Later, the flow develop and moves forward to both small horizontal and vertical scale. In the ω equation (2.13), once horizontal length scale l of the spice field becomes is smaller than length scale L of eddies, spice is no longer passive tracer and, become large and effective and w filed effects buoyancy field so as PV field. Similarly

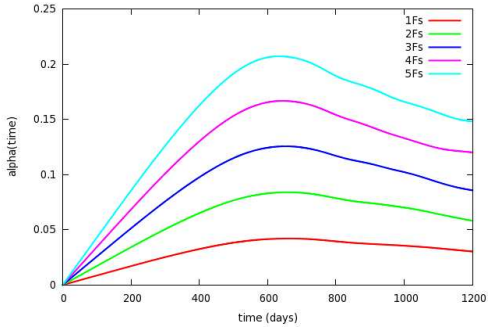

(a)

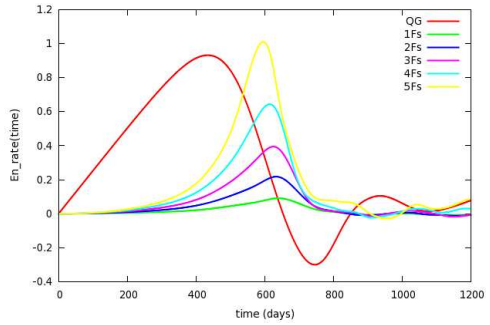

(b)

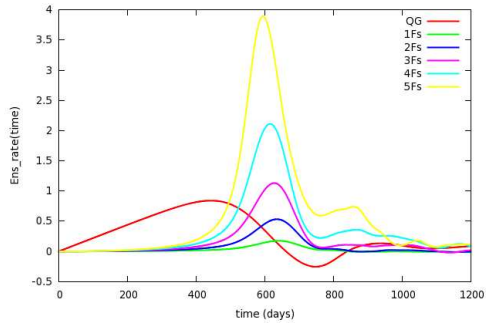

(c)

Figure 2–1: Figure 2–1(a) shows the root mean square of spice with respect to time and normalized by N_0^2. Figure 2–1(b) and 2–1(c) describe energy and enstrophy input rate with time respectivelly. Red represents rate from F and others corresponds to F_s in different spice forcing.

from equation (2.14), when vertical length scale h of spice field is small, then spice becomes important even if α_0 is small. So, in both cases, spice becomes effective at small scale. We are expecting that thermobaricity forcing can have an $O(1)$ affect on the potential vorticity field at the high wave number end of the spectrum. Let see what we do get from numerical simulation?

Figure 2–1(b) shows the transfer rate of energy from F and different spice F_s and Figure 2–1(c) describes the transfer rate of enstrophy from F and different spice F_s. In both figure, we can see that approximately upto 300 days, spice work as passive tracer i.e. there is no spice effect, and later on it plays a significant role in the simulations and continue upto 800 days, finally once anomaly is completely mixed thermobaricity becomes irrelevant. Another interesting point, although we have increased our spice forcing F_s by a factor of 1, but the effectiveness of spice is not linear. From simulations $Run-2$ to $Run-6$, we see that the contribution of spice in energy input rate goes at maximum from 10% to 110% compare to F, where as, a maximum from 40% to 400% for enstrophy rate.

Figure 2–2 represents the snapshot of potetial vorticity field of xz section at one-quarter and three-quarter in y direction for QG and MQG with different spice forcing. Small scale vertical and horizontal structures are observed in PV field after adding spice. Figure 2–2(c) and 2–2(d) are very much close to QG PV, Figure 2–2(a) and 2–2(b), field due to weak spice forcing. Adding more spice to QG turbulence can lead to an enhancement of both horizontal and vertical small scale structure in potential vorticity field (Figure 2–2(e) -2–2(h)).

Because of the vertical structure of spice forcing F_s is weakest at surface and bottom but strongest at the middle, it is normal to observe more structure at the middle.

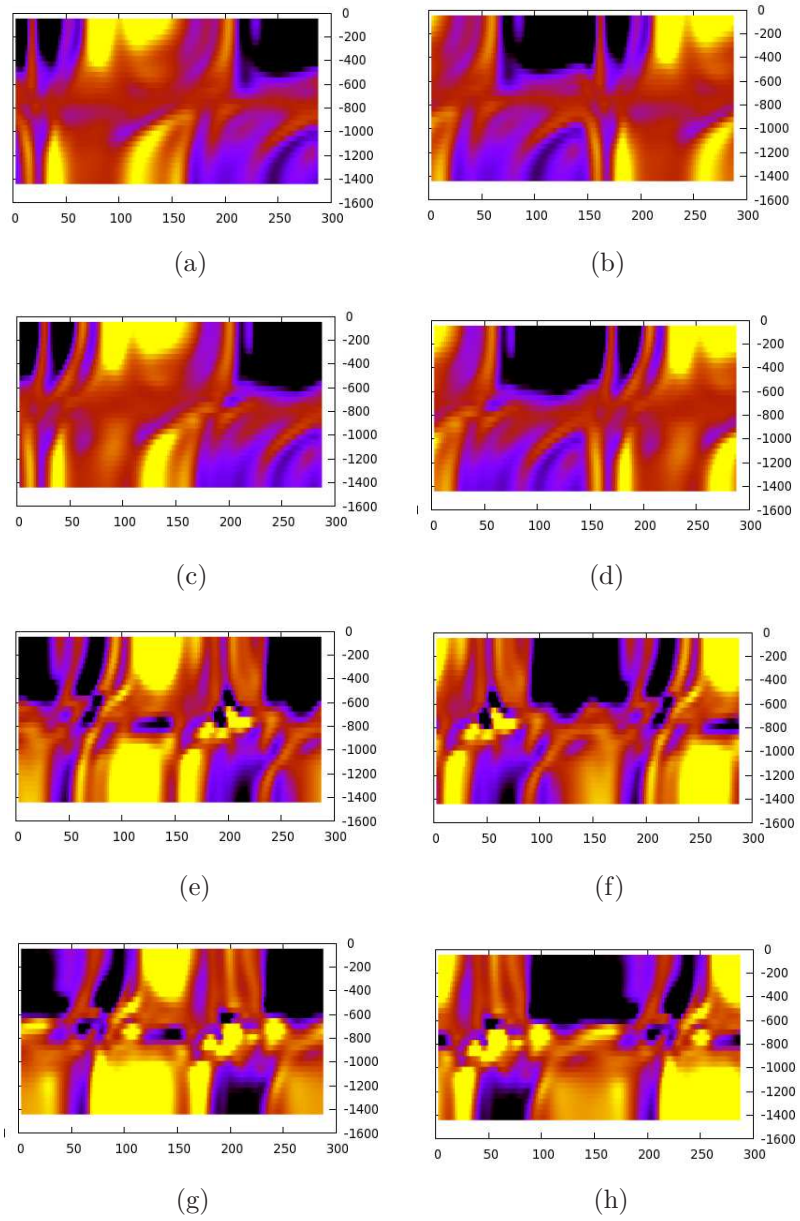

Figure 2–2: Left and right are presenting xz section of PV field at one and three quarter in y-direction respectively. QG: 2–2(a) and 2–2(b) and MQG: 2–2(c), 2–2(d); 2–2(e), 2–2(f) and 2–2(g), 2–2(h) when $\alpha = 0.04,\ \ 0.16$ and 0.2 respectively.

2.4.5 Energy and Enstrophy

The theory for QG turbulence is enstrophy is conserve which implies energy goes to upscale. With spice, both enstrophy and energy is not conserved, questions is what would be the consequence?

Figure 2–4(a) describes the flux of nonlinear term NL_{en} term in the equation (2.15). We see that energy is taken from large scales and brought it at the small scales and finally dumped. The amount of the flux at down scale are also related to spice forcing. Thus, spice forcing allows energy to cascade forward to dissipative scales. This is important since in QG dynamics energy dissipation is dominated by bottom friction at large scale.

Figure 2–4(b)shows the flux of spice forcing S_{en} term in the equation (2.15). For weak forcing, it is shown that spice effect is not significant, but the different results found when more spice forcing are added. It seems that spice forces Q_0 both at small and large scales.

Energy spectrum of QG and MQG at different vertical levels are shown in Figure 2–3. Figure 2–3(a), 2–3(b), 2–3(c) and 2–3(b) describe energy spectrum at $z = \frac{2H}{8}$, $z = \frac{3H}{8}$, $z = \frac{5H}{8}$ and $\frac{6H}{8}$ respectively. When spice forcing is large, such as $4F_s$ and $5F_s$, Figure 2–3(b) and 2–3(c) show that slope of the spectrum in MGQ is shallower than that of QG slope. As spice forces Q_0 at wide range of scale, therefore, it is expected energy to cascade upward which causes the observed shallowness of the spectrum.

2.5 Conclusion and Future Work

Due to thermobaric effect, a non-conserveness is arisen in the potential vorticity. The effect of thermobaricity on a balance dynamics, like QG, have been studied by proposing a modified version of QG (MQG) model. The model is solved numerically.

Different spice forcing are applied in different simulation. Our results suggest that the adding spice to QG turbulence can lead to an enhancement of both horizontal and vertical small scale structure in potential vorticity field. It is also observed that due to spice energy moves to dissipation scales.

High vertical resolution simulations may help to get more accurate picture of thermobaric effec, but we are constrained our computer memory. We future goal will be to convert our serial code to parallel.

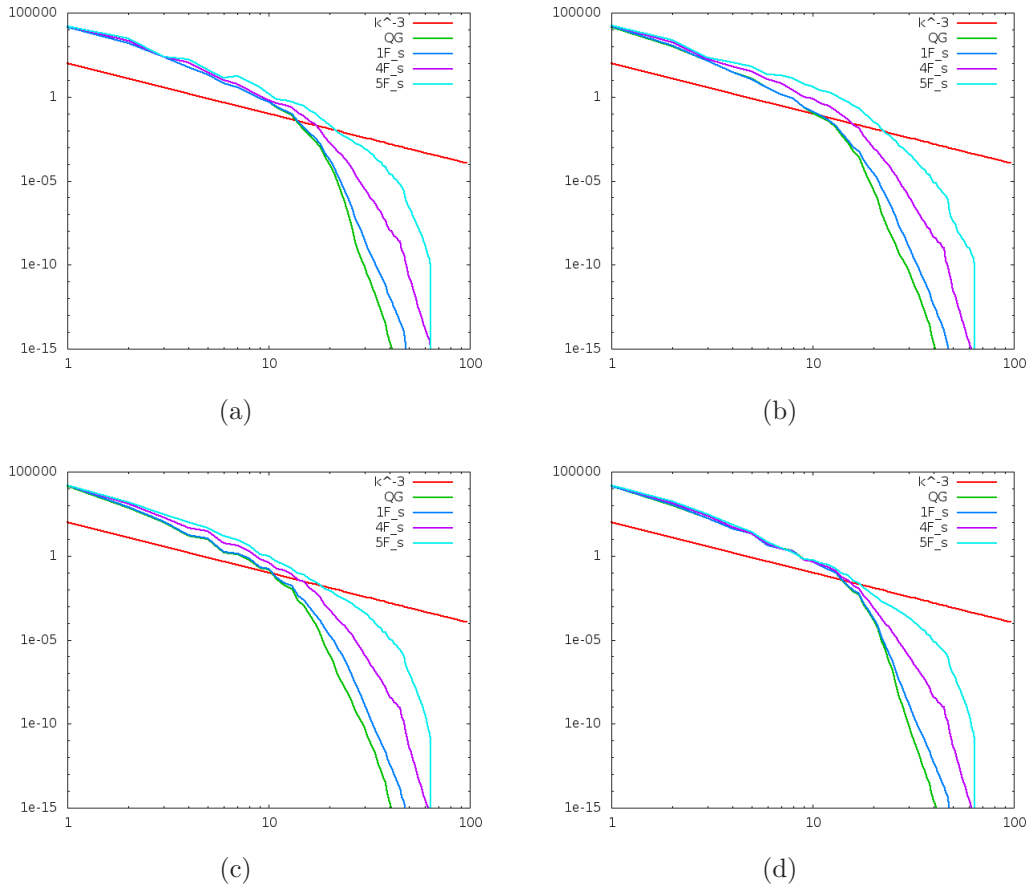

Figure 2–3: Energy spectrum of QG and MQG in different vertical level. Figure 2–3(a), 2–3(b), 2–3(c) and 2–3(d) describe at $z = 2H/8,\ 3H/8,\ 5H/8$, and $6H/8$ respectively. H = 1500 m

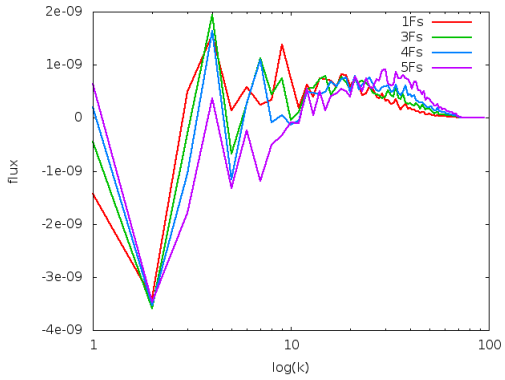

(a)

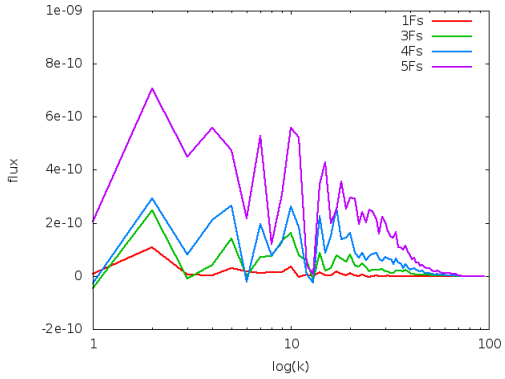

(b)

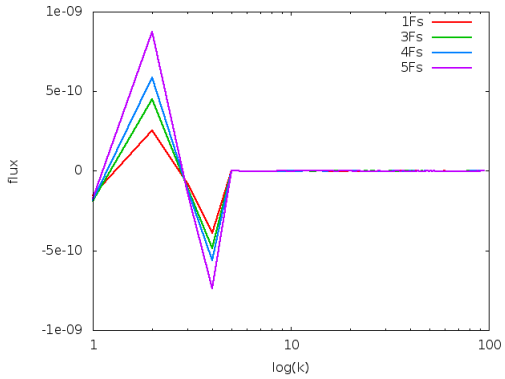

(c)

Figure 2–4: Energy flux: 2–4(a), 2–4(b) and 2–4(c) are the flux of NL_{en}, S_{en} and F_{en} respectively from the equation (2.15) . Colors are presenting different spice forcing.

CHAPTER 3
Jets and β-plane Turbulence

3.1 Introduction

Two-dimensional (2D) or barotropic flow has been evaluated in many previous studies to form zonal jets ([1], [5]). Recently, three dimensional structures of the jets have been found by analyzing Agro data collected between 2004 and 2006 [10] but the effects of this structures are still not well understood. Figure 3–1(a) and 3–1(b) represent the horizontal and vertical cross section of time average zonal velocity respectively.

Rhines [1] first theorized the eddy timescale increases as the spatial scale grows in the inverse cascade, therefore, a transition will occur at the spatial scale where the eddy timescale matches that of Rossby waves with the same spatial scale. The transition scale, commonly referred to as the *Rhine's scale*, is $L_\beta \sim \sqrt{U/\beta}$, where U is the square root of the eddy kinetic energy. Barotropic upscale energy cascade is halted by β at wavenumber κ_β. Vallis and Maltrud [5] refined the idea and insted of one dimentional isotropic spectra, he presented a 2 dimensional dumbbell-shaped spectra centred along wavenummber κ_x. As jets are not barotropic, so the vertical structure also may play a role to change the shape of the dumbbell which is still unknown. We are proposing Surface Quasigeostrophic (SQG) model for β -plane turbulence to get better understanding the role of vertical structure in jets.

A brief review of β plane turbulence is presented in Sction 3.2. Section 3.3 describes SQG models and a comparison between SQG and bartopic jets will be shown in section 3.4.

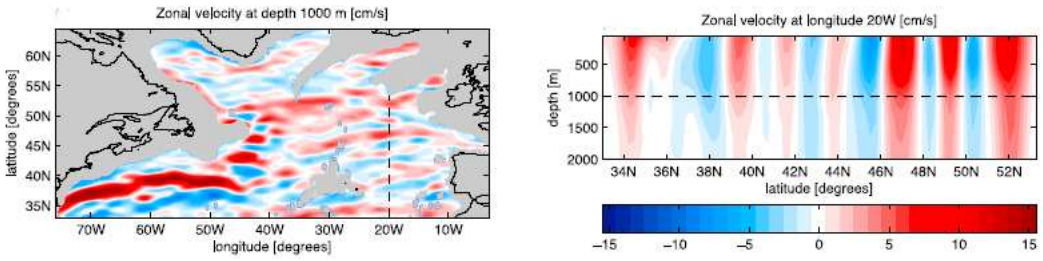

(a) (b)

Figure 3–1: Evidence of quasi-zonal jets in the Argo data for 2004 through 2006: 3–1(a) the map of zonal velocity at 1000 m shows many zonally elongated areas of eastward and westward velocity. Areas shaded gray are deeper than 2000 m, where no data is available. 3–1(b) A vertical cross section at 20W of the same data shows that the alterations of positive and negative velocity are vertically coherent and reach to depths of more than 2000 m. Collected from [10]

3.2 β-plane turbulence

Variations in the Coriolis parameter with latitude caused by planetary curvature affects geophysical flows by introducing an anisotropy that results in the spontaneous generation of zonal jets.

3.2.1 Scaling of β-plan turbulence

The scale where the β-effect become important, k_β, has been a source of controversy and confusion for the past 20 years. Rhine [1] first introduced from the vorticity equation

$$\underbrace{\frac{\partial}{\partial t}}_{\frac{U}{LT}}\zeta + \underbrace{\mathbf{u}\cdot\nabla\zeta}_{\frac{U^2}{L^2}} + \underbrace{\beta v}_{\beta U} = 0, \tag{3.1}$$

at large scales the β-term dominates, and smaller scale the advective term dominates, so there is a cross-over scale, L_β, called *Rhines scale* is given

$$L_\beta = \sqrt{\frac{U}{\beta}}; \quad k_\beta = \sqrt{\frac{\beta}{U}}$$

Here, L_β is a natural length scale arising from β and a velocity scale U, where Rhines [1] takes U to be the total r.m.s of velocity, including both zonal and eddy components of the flow. Rhines further suggests that β halts the barotropic inverse cascade at wavenumber $k_\beta = L_\beta^{-1}$. Followed by the Rhines, Vallis and Maltrud [5] suggested that two-dimensional spectra can be exhibit a dumbbell-shaped region centered along the x-axis insted of an isotropic spectrum.

3.2.2 Vallis and Maltrud

It is expected that turbulence would excite Rossby waves when the wave frequency ω and inverse of eddy turnover time τ^{-1} are matched.

$$\omega \sim \tau^{-1}; \qquad \tau = \left[\kappa^3 E(k)\right]^{\frac{1}{2}} \tag{3.2}$$

Vallis and Maltrud [5] calculated k_β from the energy cascade rate ϵ and β. There expression

$$\frac{\beta k^x}{\kappa^2} = \left[\kappa^3 \epsilon^{2/3} \kappa^{-5/3}\right]^{\frac{1}{2}} = \kappa^{2/3} \epsilon^{1/3} \tag{3.3}$$

Using polar coordinate system, we can separate x and y component of wavenumber k. So, $k_\beta^x = r\ cos(\theta)$ and $k_\beta^y = r\ sin(\theta)$ and $\kappa = \sqrt{(k_\beta^x)^2 + (k_\beta^y)^2} = r$, where $\theta = tan^{-1}\left(\frac{k^x}{k^y}\right)$. We get

$$r = \left(\frac{\beta^3}{\epsilon}\right)^{1/5} cos^{3/5} \tag{3.4}$$

and therefore

$$k_\beta^x = \left(\frac{\beta^3}{\epsilon}\right)^{1/5} cos^{8/5}(\theta); \quad k_\beta^x = \left(\frac{\beta^3}{\epsilon}\right)^{1/5} cos^{3/5}(\theta)\ sin(\theta) \tag{3.5}$$

3.2.3 Holloway and Hendershott

Holloway and Hendershott [4] offer a third possibility for k_β, where now the balance is between β and the r.m.s of barotropic vorticity

$$\frac{\beta k^x}{\kappa^2} = \bar{\zeta} \tag{3.6}$$

and their dumbbell

$$k^x_\beta = \left(\frac{\beta}{\bar{\zeta}}\right) cos^2(\theta); \quad k^x_\beta = \left(\frac{\beta}{\bar{\zeta}}\right) cos(\theta)\ sin(\theta) \tag{3.7}$$

3.2.4 Rhaines expression

The Rhines expression for dumbbell would be;

$$\frac{\beta k^x}{\kappa^2} = \left[\kappa^2 \kappa E(k)\right]^{\frac{1}{2}} = \kappa U \tag{3.8}$$

and

$$k^x_\beta = \left(\frac{\beta}{U}\right)^{1/2} cos^{3/2}(\theta); \quad k^x_\beta = \left(\frac{\beta}{U}\right)^{1/2} cos^{1/2}(\theta)\ sin(\theta) \tag{3.9}$$

These three length scales are all distinct, and further ambiguity arises as to whether the velocity U and vorticity ζ scales should be comprised of eddy components, zonal components or both.

Although, the both zonal and meridional component of κ_β look different, but there are no qualitative change among their dumbbell, so we will compare our scale with Rhines scale only.

3.3 SQG and diagnostics

SQG model has buoyancy evolution at the surface with zero potential vorticity (PV) interior. The SQG equations with β

$$\frac{D}{Dt}\psi_z^s = 0; \quad at \quad z = H; \quad \psi_z^b = 0, \quad at \quad z = 0 \tag{3.10}$$

$$Q = 0; \quad 0 \leq z \leq H \tag{3.11}$$

where $Q = \nabla^2\psi + \frac{f^2}{N^2}\frac{\partial}{\partial z}\psi_z + \beta y$ and s and b represent upper and bottom surface respectively. We can split Q,

$$Q = \bar{Q} + Q' \tag{3.12}$$

where $\bar{Q} = \nabla^2\Psi + \frac{f^2}{N^2}\frac{\partial}{\partial z}\Psi_z + \beta y = 0$, implies that $\Psi_{zy} = U_z = -\frac{\beta N^2 z}{f^2}$, and $Q' = \nabla^2\psi' + \frac{f^2}{N^2}\frac{\partial}{\partial z}\psi'_z = 0$ and we can rewrite the equations (omitting prime) in the form

$$\frac{D}{Dt}\psi_z^s + U^s\frac{\partial}{\partial x}(\psi_z^s) - \frac{\beta N^2 H}{f^2}\frac{\partial \psi^s}{\partial x} = 0; \quad at \quad z = H \tag{3.13}$$

$$Q = 0; \quad 0 \leq z \leq H \tag{3.14}$$

$$\psi_z^b = 0; \quad at \quad z = 0 \tag{3.15}$$

The analytic solution for ψ and ψ_z from Q

$$\hat{\psi} = \frac{H}{\mu}\frac{\cosh\left(\frac{\mu}{H}z\right)}{\sinh(\mu)}\hat{\psi}_z^s \tag{3.16}$$

$$\hat{\psi_z} = \frac{\sinh\left(\frac{\mu}{H}z\right)}{\sinh(\mu)}\hat{\psi}_z^s \tag{3.17}$$

where $\mu = \frac{NH\kappa}{f}$. The relationship between $\hat{\psi}$ and $\hat{\psi_z}$ at surface,

$$\hat{\psi} = \frac{H}{\mu}\frac{\hat{\psi_z^s}}{\tanh(\mu)} \tag{3.18}$$

At large scale, $\mu \ll 1$ and $\tanh(\mu) \to \mu$, then the temperature is related to the streamfunction like $\hat{\psi}_z^s = H^{-1}\mu^2\hat{\psi}^s$, while at small scale, $\mu \gg 1$ and $\tanh(\mu) \to 1$, the inversion is approximately $\hat{\psi}_z^s = H^{-1}\mu\hat{\psi}^s$. Thus the relation between the streamfunction and the advected temperature transitions from a 2D-like inversion at large scales, to an SQG-like inversion at small scales, with the transition occurring at the wavenumber $\mu \sim 1$ (i.e., at the deformation wavenumber).

3.3.1 Dumbbell Shape Spectra for SQG

The dispersion relationship form SQG model is ($U = 0$)

$$\omega_{SQG} = -\frac{\beta k^x NH}{\kappa f \ \tanh(\mu)} = -\frac{\beta k^x}{\kappa^2}\frac{\mu}{\tanh(\mu)} = \omega_{2D}\frac{\mu}{\tanh(\mu)} \tag{3.19}$$

In SQG, total energy is sum of kinetic and potential energy, to compare with 2D dumbbell, we need to calculate kinetic energy from total energy, say $E_{2D} = \alpha(k)E(k)_{SQG}$, then

$$\tau = \sqrt{\alpha(\kappa)}\left[\kappa^3 E(k)_{SQG}\right]^{\frac{1}{2}} \tag{3.20}$$

where $\alpha(\kappa) = \frac{1}{1+\tanh^2(\mu)}$. The shape of the dumbbell

$$-\frac{\beta k_x}{\kappa^2}\frac{\mu}{\tanh(\mu)} = \sqrt{\alpha(\kappa)}\ \kappa U \tag{3.21}$$

At the large scale, $\tanh(\mu) \sim \mu$, and $\alpha \sim 1$, therefore, we can recover two-dimensional dumbbell and for small scale, $\tanh(\mu) \sim 1$, and $\alpha \sim 0.5$, a different shape would be found. Barotropic and SQG dumbbell are compared in Figure 3–2. Clearly, in the real ocean stratification qualitative change between barotropic and SQG dumbbells is observed.

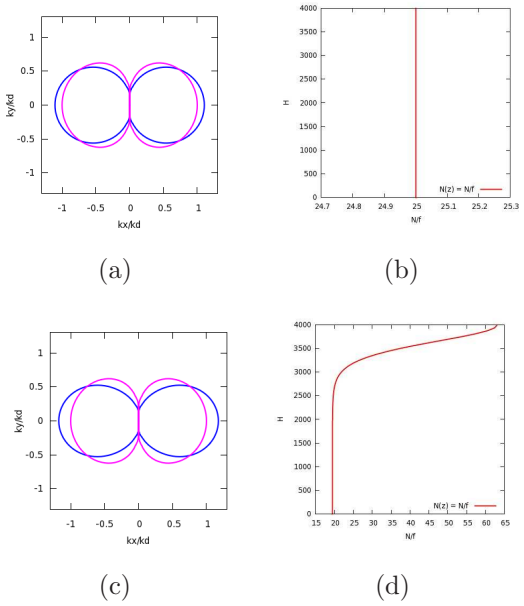

Figure 3–2: Barotropic (pink) and SQG (blue) dumbbell are compared. First row: $N(z)$ = constant. 2nd Row: $N(z) \neq$constant.

3.4 Numerical Simulations

Numerical simulations of barotropic and SQG jets with $N(z)$ is constant and non-constant are presented. Buoyancy frequency $N = 25 \times f$, Coriolis parameter $f = 1 \times 10^{-4}$, and $H = 4\ km$ is depth are considered. The Rossby deformation radius is evaluated as $k_d = L_d^{-1} = 15 \times \kappa$, where $\kappa = \frac{2\pi}{L}$ is wavenumber and L is horizontal domain size. We put the initial energy E_0 at wave $\kappa_{input} = 2\kappa_d$

The horizontal resolution of the simulation is $k_{max} = 256$ or $nx \times ny = 512 \times 512$ resolution in grid space. For time integration, we have used finite difference technique, second order accuracy Leap-frog scheme, and Robert-Asselin filter 0.01 is used. When N is constant, to invert ψ field numerically, we transform from ψ_z real space to Fourier space $\hat{\psi}_z$, then the analytic solution of $\hat{\psi}$ is used and then get back to real space. All the transformation is done with the help of Fast Fourier

Transformation (FFT). When $N(z)$ is not constant, Shooting method is applied to get vertical structure of $\hat{\psi}$ and $\hat{\psi}_z$ wave-number (k^x, k^y) wise.

3.4.1 Dumbbell

Why is the shape of the dumbbell important? We are solving initial value problem and so initially we put our energy at isotropic region where β effect is negligible, then energy migrates across the (k^x, k^y) plane. As the energy approaches the waveturbulence crossover β becomes effective and it starts to pile up at the boundary and penetrates the wave-dominated region only very slowly. In crossover boundary wave dominated region blocks energy to migrate farther inside, however, energy migrates towards the k^y axis is not blocked. The interesting question is here, how far it can go, because it measures the width of the jets i.e. length scale.

Dumbbell of barotropic and SQG jets are presented in Figure 3–3. Changes between barotropic (Figure 3–3(a) and 3–3(b)) and SQG (Figure 3–3(c) and 3–3(d)) dumbbell are observed but not significant. However, a qualitative difference is observed when real ocean stratification is considered in Figure 3–3(e) and 3–3(f). It is also shown that the energy pushes toward smaller k^y compare to barotropic flow. Therefore, we will observe wider jets compare to barotropic jets.

3.4.2 Zonal Velocity

Figure 3–4(a), 3–4(b) and 3–4(c) describe the zonal velocity of barotropic, SQG constant and non constant stratification respectively. Vertical structure of zonal velocity is presented in Figure 3–4(d). It shows clearly the wider jets in SQG dynamics that was expected.

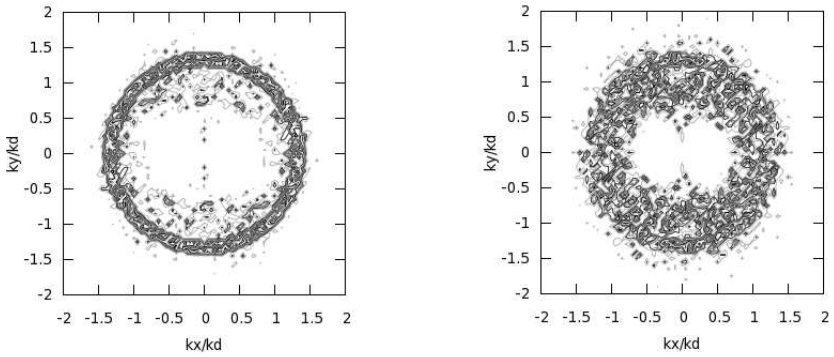

(a)

(b)

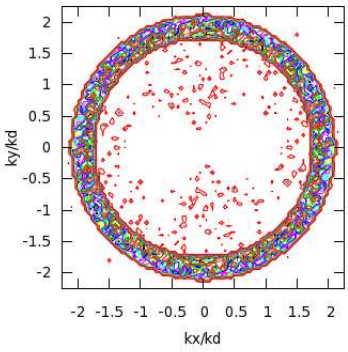

(c)

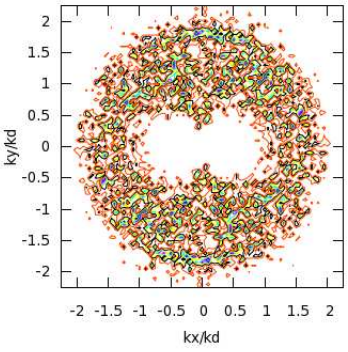

(d)

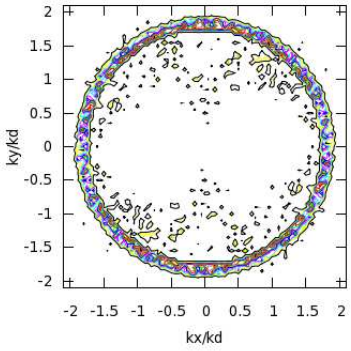

(e)

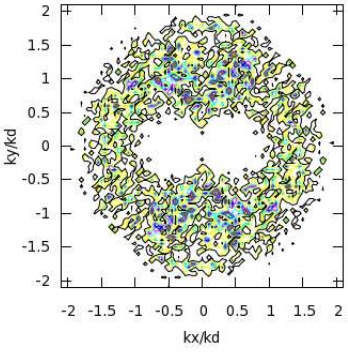

(f)

Figure 3–3: Dumbbell shape of kinetic energy. Barotropic dumbbell : Figure 3–3(a) and 3–3(b). SQG dumbbell : Figure 3–3(c), 3–3(d) and SQG dumbbell with real ocen stratification : Figure 3–3(e), 3–3(f).

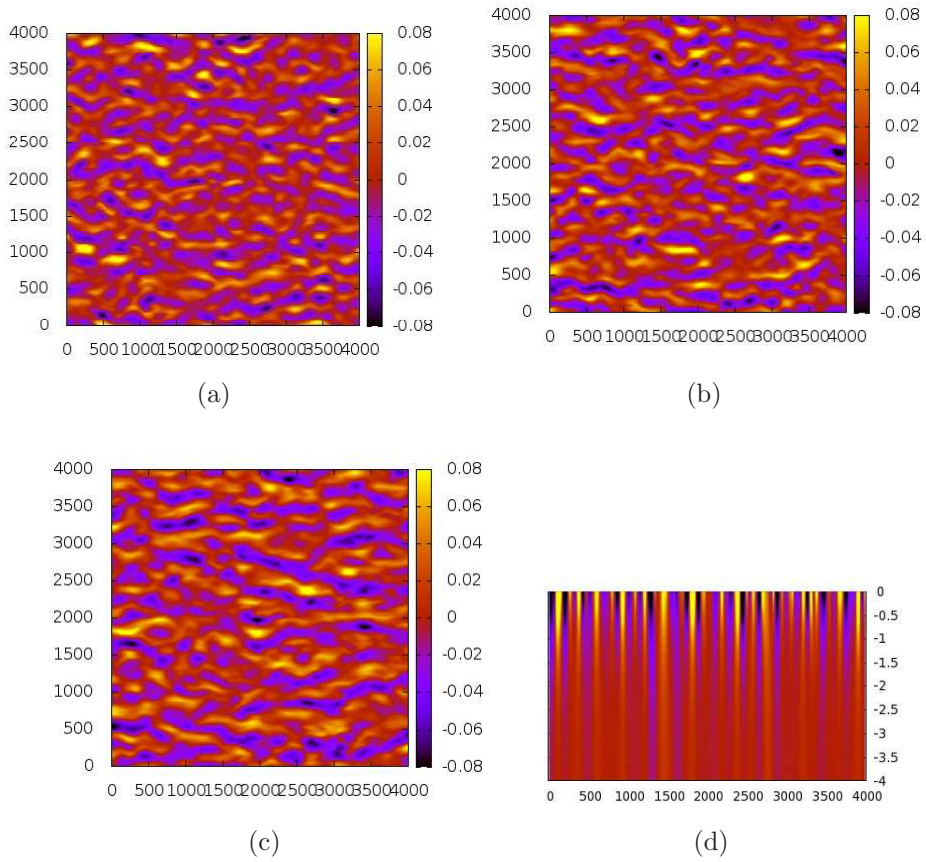

Figure 3–4: Zonal velocity of jets. 2D jets: Figure 3–4(a), SQG: Figure 3–4(b) SQG when N = constant and SQG: Figure 3–4(c) when $N \neq$ constant. 3–4(d) represents vertical structure of jet (N = constant).

3.5 Conclusion and Future Work

Jets in the ocean are not a barotropic flow and it has three dimensional structure. A surface quasigeostropic model in β plane is proposed. We have found that the vertical structure change the length scale of jets.

SQG dynamics does not create Q in interior, and extension of this work will be regular QG model including surface buoyancy.

References

[1] Rhines B. Waves and turbulence on β-plane. *Journal of Fluid Mechanics*, 69:417–443, 1975.

[2] Straub D. On thermobaric production of potential vorticity in the ocean. *Tellus*, 51A:314–325, 1998.

[3] Charney G. Geostrophic turbulence. *Journal of the Atmospheric Sciences*, 28:1087–1095, 1971.

[4] Holloway G and Hendershott M. Stochastic closure for nonlinear rossby waves. *Journal of Fluid Mechanics*, 82:747–765, 1977.

[5] Vallis G and Maltrud M J. Generation of mean flows and jets on a beta plane and over topography. *Journal of Physical Oceanography*, 23:1346–1362, 1992.

[6] Akitomo K. Open-ocean deep convection due to thermobaricity. 1. scaling argument. *Journal of Geophysical Reasearch*, 104:5225–5234, 1999.

[7] Fu L and Flierl G. Nonlinear energy and enstrophy transfers in a reealistic stratified ocean. *Dynamics of Atmospheric and Oceans*, 4:219–246, 1980.

[8] Salmon R. Baroclinic instability and geostrophic turbulence. *Geophysical and Astophysical Fluid Dynamics*, 15:167–211, 1980.

[9] Lindzen S and Fox-Rabinovitz M. Consistent horizontal and vertical resolution. *Monthly Weather Reveiw*, 117:2575–2583, 1989.

[10] Kamenkovich I Sebille E and Willis J. Quasizonal jets in 3d argo data of the northeast atlantic. *Geophysical Reasearch Letters*, 38:L02606, 2011.

[11] McDougall T. Thermobaricity, cabbeling, and water-mass conversion. *Journal of Geophysical Reasearch*, 92:5448–5464, 1987.